Int J Earth Sci (Geol Rundsch) (2017) 106:2855–2872
DOI 10.1007/s00531-017-1463-z

ORIGINAL PAPER

Cooling history of nested plutons from the Variscan Tichka plutonic complex (Morocco)

Christophe Lécuyer[1,4] · Dominique Gasquet[2] · Pascal Allemand[1] · François Martineau[1] · Isabelle Martinez[3]

Received: 23 May 2016 / Accepted: 12 February 2017 / Published online: 12 March 2017
© Springer-Verlag Berlin Heidelberg 2017

Abstract Four imbricated mafic to felsic plutons of Variscan age from Morocco have been investigated for their cooling history and geochemical interactions with surrounding continental rocks. Oxygen isotope compositions of whole rocks and minerals have been used to model the cooling rates of these kilometer-sized intrusions. By combining both the knowledge of oxygen-self diffusion data of rock-forming minerals and the determination by IR-spectroscopy of the water content of quartz, the cooling times are estimated ranging from 10^5 to 5×10^5 years in agreement with the shallow emplacement (4–6 km depth) of these intrusions into the continental crust. Such fast cooling rates could explain why after assimilation of the various country rocks, heterogeneities of both neodymium and strontium isotope ratios were still preserved. A progressive $\delta^{18}O$ increase from the mafic to felsic terms of the plutonic suite, which does not excess 1 to 1.5‰, could be explained by the assimilation of metamorphosed pelitic and volcanic rocks that constitute the basement of the Tichka plutonic complex.

Keywords Variscan orogeny · Crustal growth · Cooling rate · Oxygen isotopes · Tichka massif · Morocco

Introduction

The role of aqueous fluids upon magma genesis and subsolidus evolution of plutons has been investigated for decades (e.g., Chappell 2004; Ballouard et al. 2015 and references therein). The cooling rates of plutons may also influence the processes of magma mixing, chemical, and isotopic exchange between different rock suites (see Bando et al. 2003; Annen et al. 2006; Barboni et al. 2013, 2015). The Tichka plutonic complex (TPC) displays a close association of coeval unaltered plutonic rocks with a broad spectrum of geochemical compositions. Therefore, we combined several methods to decipher the cooling history of these plutons, which are (1) granulometric and modal data of the various rock types, (2) an oxygen isotope study of whole rocks and their forming minerals, and (3) a determination of water contents of quartz determined by IR-spectroscopy.

Moreover, the combination of stable isotope measurements with previously published Sr and Nd isotope data (Gasquet et al. 1992) should better constrain the proportion and the composition of the contaminant material. It is generally admitted that aqueous fluids are required to promote partial melting of the continental crust. Stable isotope studies of the melting products have the potential to determine the source and the amounts of these aqueous fluids (e.g. Taylor 1968, 1977, 1988; Wickham and Taylor 1987; Johannes and Holtz 1996). These fluids may come from

✉ Christophe Lécuyer
clecuyer@univ-lyon1.fr

Dominique Gasquet
dominique.gasquet@univ-savoie.fr

1 Laboratoire de Géologie de Lyon, CNRS UMR 5276, Bâtiment Geode, Campus de la Doua, Université Claude Bernard Lyon 1, 27-43 Boulevard du 11 Novembre 1918, 69622 Villeurbanne Cedex, France

2 Laboratoire-EDYTEM (Environnements, Dynamiques et Territoires de la Montagne), CNRS UMR 5204, Université de Savoie-Mont Blanc, Campus scientifique, 73376 Le Bourget du Lac Cedex, France

3 Laboratoire de Géochimie des Isotopes Stables, I.P.G.P., Université Paris VII, 2 Place Jussieu, 75251 Paris Cedex 05, France

4 Institut Universitaire de France, Paris, France

external reservoirs in the context of rifting (seawater) and subduction, or continental collision (meteoric waters) (e.g., Taylor 1988 and references therein; Ruano et al. 2002; Zak et al. 2005; Ballouard et al. 2015). They can also be recycled through dehydration of previously hydrated wall-rocks at the pluton roots (e.g., Fourcade and Allègre 1981; Gazis et al. 1995).

The TPC presents a remarkable coeval suite of four mafic-to-felsic magmatic intrusions of Variscan age (Termier and Termier 1971; Vogel and Walker 1975; Gasquet 1992; Gasquet et al. 1992). This massif has been recognized as an excellent example to test how a mafic to felsic magmatic suite may be generated and incorporated into the continental crust. Consequently, we consider the TPC as an adequate example to perform stable isotope measurements and thermal modeling. The previous studies of the complex have shown that the mafic and felsic end-members derived from various rock sources (Scott and Vogel 1980; Gasquet et al. 1992). A model of assimilation and fractional crystallization (AFC) (Taylor 1980; De Paolo 1981; Smith et al. 1999; Van de Flierdt et al. 2003; Wu et al. 2003) dominated by a strong mantellic component and melting of mafic to intermediate heterogeneous continental sources was retained as the most likely scenario to explain the occurrence of mafic (gabbros), intermediate (diorites), and felsic (granodiorites to monzogranites) members (Gasquet et al. 1992). The melting of the various sources is linked to a large-scale tectonothermal process as identified elsewhere in other granitoid suites (e.g., Creaser 1996; Van De; Flierdt et al. 2003; Christofides et al. 2007, among others) or recently modelized by Annen et al. (2015).

Geological setting

The TPC crops out 120 km SW of Marrakech in the Western High Atlas (Morocco). It was intruded 291 ± 5 Ma ago (Gasquet et al. 1992) close to the South Atlasic Fault (Fig. 1), in Lower Cambrian volcano-sedimentary sequences. These wall-rocks, mainly consisting of

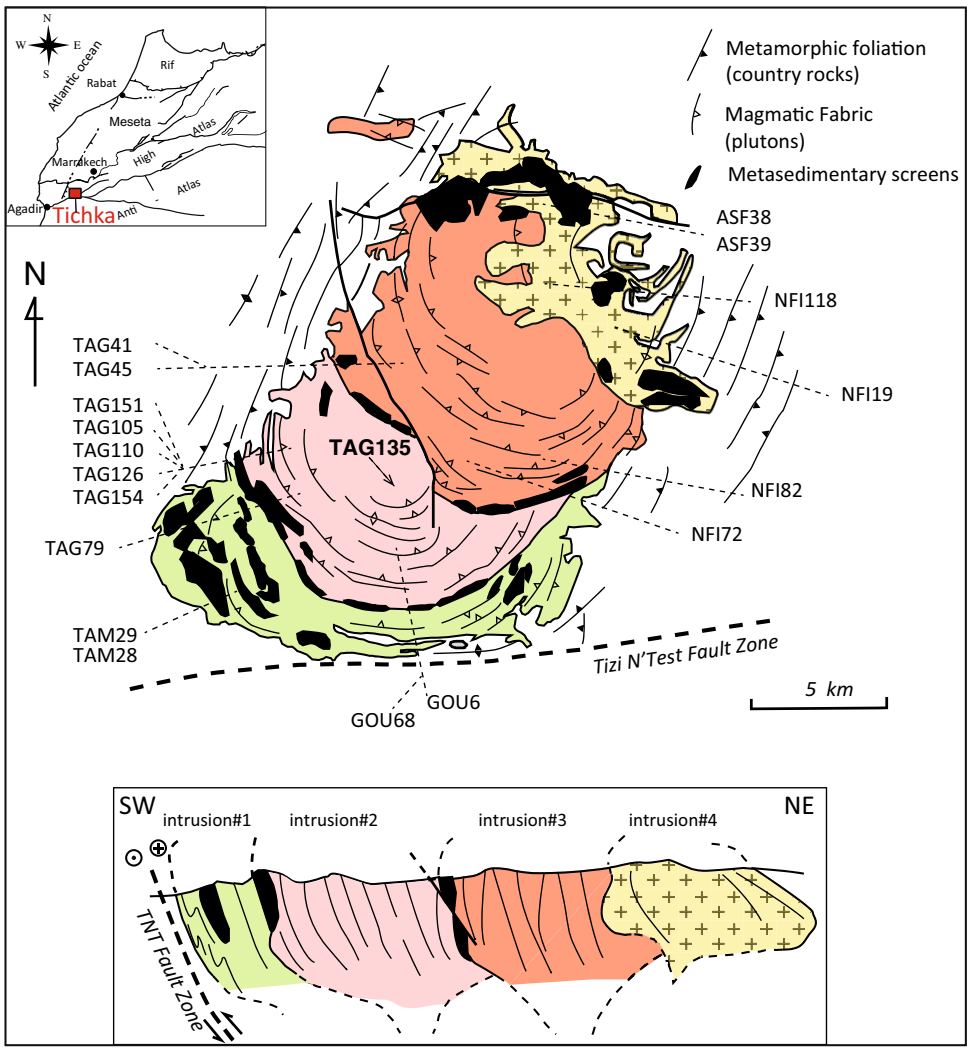

Fig. 1 Schematic map and cross section of the four nested Tichka intrusions along with the location of studied samples. Because of the poorly defined geometry of intrusion#4 on the map, only the external contour of this intrusion was drawn. It must be noted that sample NFI118 crops out in a window of intrusion#3 within intrusion#4

andesites, rhyolites, tufs, pelites, and carbonates, were metamorphosed in the greenschist facies. A systematic structural study showed that the Tichka plutonic complex is made of four nested intrusions, limited by screens of metasediments from the country rocks and displaying unconformable magmatic fabrics (Gasquet 1992; Gasquet et al. 1992; Fig. 1). On the basis of field observations and wihout detailed and recent geochronological data, it is assumed that the three southwestern intrusions, which have composite lithologies ranging from gabbros to leucomonzogranites, were formed sub-contemporaneously, while the northeastern intrusion is made of leucogranitic discontinuous and irregular pods, and was emplaced slightly later (Gasquet 1992).

The pluton is supposed built by ballooning and to be the result of in-situ assemblage of four magma batches which were injected into pre-existing country rocks in relation to transpressional tectonic regime (Lagarde and Roddaz 1983) as well demonstrated in similar plutonic complexes (Wang et al. 2002; Asrat et al. 2003; Glazner et al. 2004; Matzel et al. 2006; Barbey et al. 2008; Clemens et al. 2009). In each intrusion, five major rock types are present: (1) gabbros, (2) diorites, (3) granodiorites-tonalites, (4) monzogranites, and (5) leucogranites. In the two most southern intrusions, diorites and granodiorites are closely associated defining a "zebra structure" (Termier and Termier 1971) and represent about 35% of the intrusion volume (Fernandez and Gasquet 1994). This "zebra structure", which marks the magmatic relationships between diorite and granitoid intrusions, is characterized by sharp and lobate contacts clearly indicating the coeval character of the two magmas (Vogel and Walker 1975; Wiebe and Collins 1998; Collins et al. 2000; Christofides et al. 2007) without apparent important mixing during their emplacement. In the northern part of the massif, the diorites mainly occur as scattered enclaves ranging in size from 1 m to more than 10 m. Enclaves and intrusions of diorites have a similar mineralogy, but large variations in grain size (less than 1 mm up to 5 mm), texture (subdoleritic to intergranular), and in modal proportions.

Gabbros have fine-to-medium-grained ophitic textures and constitute hectometric lenses with sharp contacts in the presence of diorites. These gabbros are composed of olivine, augite, labradorite, calcic amphibole (kaersutite to magnesio-hornblende), hypersthene, and small amounts of phlogopite and ilmenomagnetite. Diorites occur as large intrusions that alternate with granitoid strips (the so-called "zebra structure"). The common mineral assemblage is made of plagioclase (oligoclase-andesine), magnesio-hornblende, biotite, titanite, and ilmenite, while interstitial quartz and K-feldspar occur in the most evolved members. The granodiorites–tonalites are in volume the dominant plutonic rocks of the massif. They are coarse-grained and composed of oligoclase, hornblende, biotite, quartz, and K-feldspar with minor amounts of titanite, allanite, ilmenite, and apatite. The monzogranites also display sharp lobate or progressive contacts with associated granodiorites highly suggesting a synmagmatic emplacement as for the diorite-granodiorite association. These equigranular monzogranites include rare and small quartz-dioritic enclaves. They are made of quartz, K-feldspar, oligoclase, biotite, and hornblende with minor amounts of titanite and ilmenomagnetite. The leucogranites occur in dykes or large stocks that crosscut the granitoids described above. They constitute the last intrusive event, especially represented in the northeastern part of the TPC. We can distinguish two subgroups (1) biotite ± amphibole leucomonzogranites (samples NFI72 and ASF38) associated with the monzogranites and (2) two-micas leucogranites (samples ASF39 and NFI118) with rare andalusite, garnet, and cordierite, and that crosscut all the other rock types.

Secondary alteration of rocks Even if the plutonic rocks constituting the TPC are remarkably unaltered, locally some samples show secondary minerals (see Gasquet 1991, for more details). Fine-grained secondary muscovite develops in facies as sericite inclusions in feldspar, as small grains around coarse primary muscovite (leucogranites). Furthermore, some biotites as well as rare amphiboles are chloritized, rare plagioclase being alibitized. These alterations are visible at the microscopic scale and are localized at the contact with country rocks or with metasedimentary screens within the massif suggesting late hydrothermal circulations of fluids. The post-solidus deformation event is evidenced by plastic deformation marked by recrystallized quartz and feldspar aggregates surrounding deformed residual phenocrysts of K-feldspar and plagioclase. Furthermore, mylonitic foliations are present in a few local zones in the TPC and more especially in the southern part of the complex where a discontinuous pluri-hectometric-wide zone can be seen from East to West along the Tizi N'Test fault Zone (Lagarde and Roddaz 1983; Gasquet 1992).

According to their chemical compositions, the Tichka plutonic rocks have been classified in three main magmatic associations found with the same chemical signatures in the three southern intrusions of the TPC; the northern fourth intrusion being composed almost exclusively of leucogranites (Fig. 2 and Gasquet et al. 1992, 1996):

- a medium-K calc-alkaline association composed of gabbros, diorites, tonalites, granodiorites, and monzogranites,
- a high-K calc-alkaline association composed of monzogabbros, monzodiorites, and biotite ± hornblende leucomonzogranites,
- a high-K calc-alkaline to shoshonitic association mainly composed of peraluminous two-micas leucogranites.

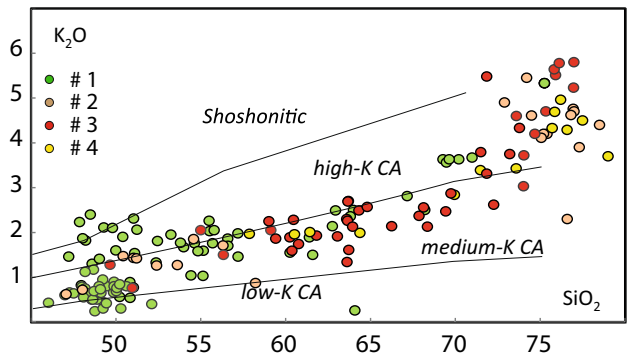

Fig. 2 K_2O versus SiO_2 (wt%) diagram for the rocks from the four intrusions (see figure for symbol coulors and intrusions)

Major and trace element data together with Rb-Sr and Sm-Nd isotopes rule out any genetic process involving a unique homogeneous source for the different magmas (Gasquet et al. 1992). Indeed, the Sm–Nd isotopic heterogeneity implies the existence of contrasting source rocks and the combination of different mechanisms. The gabbro and diorite magmas are assumed to derive from the melting of a depleted upper mantle source, whereas a combined wall-rock assimilation-fractional crystallization (AFC) model has been proposed for the evolution of the diorite suite. In contrast, the granitoids are mainly the result of the anatexis of a dominant basic to intermediate igneous heterogeneous continental crust and the two-mica leucogranites result from the partial melting of continental sedimentary rocks (Gasquet et al. 1992).

Analytical techniques

Mineralogy

The modal and granulometric analyses of Tichka samples are presented in Tables 1 and 2, respectively. They have been performed on thin sections with a videographic interactive analyser developed by Lapique et al. (1988). Uncertainty is about ±0.2%.

A minimal abundance of about 5 wt% made possible the separation of mineral fractions for isotopic analysis using successively, heavy liquids, a Frantz™ electromagnet, and hand-picking (Table 1). The quality of mineral fractions was then checked by X-ray diffractometry, and mineral concentration is certified to be equal or higher than 98 wt%.

Transmission electronic microscopy (TEM)

Thin sections (30 µm) were prepared using a thermosensitive resin. Selected areas were then cut and sandwiched between copper grids. Sample TAG126 from intrusion#2 was selected as representative for three main reasons: (1) its unaltered mineralogy, (2) its richness in quartz in which water could be more easily tracked, and (3) mineral proportions and $\delta^{18}O$ of both whole rock and mineral separates are available. This sample was thinned in an argon ion mill to be transparent to electrons. We used a JEOL 2000 EX TEM operating at 200 kV in the conventional and scanning transmission electron mode (STEM), equipped with a Tracor TN 5400 energy dispersive X-ray microanalyser.

Infrared spectroscopy

Infrared absorption was measured by Fourier transform infrared (FTIR) spectroscopy on double polished sections (250–300 µm) using an infrared microscope (Spectra Physics/Nicolet 550 m) to focus the beam down to 50 µm. Water absorbs both in the IR (infra red) and NIR (near infra red) region, giving rise to both sharp peak or broadband, each of them being assigned either to molecular water or to OH^-, respectively. Most commonly, the conventional IR spectra are used to quantify water (OH and H_2O) in glasses or minerals (e.g., Jendrzejwski et al. 1996), whereas NIR is used to determine water speciation. In this study, we used the broad-band absorption between 2500 to 4000 cm^{-1} to determine water content in quartz, without any distinction between the different forms of incorporation. IR spectra were recorded with a resolution of 4 cm^{-1}, the perturbation caused by atmospheric water was corrected by subtracting a blank spectrum collected without sample. Figure 3a shows two spectra obtained by analyzing two quartz grains from monzogranite TAG126. To quantify the broadband due to water absorption, we subtracted the background that was modeled by a curved line between 2500–4000 cm^{-1}, as shown in Fig. 3b. In some cases, we tested the sensitivity of the calculation to the choice of the baseline using different baselines (Table 3). Then, the area was measured and the Beer–Lambert law (1) was applied according to the following:

$$c = \frac{\Delta}{Ie} \quad (1)$$

where c is the total water concentration in mole H l^{-1}, Δ is the measured absorption in cm^{-2}, e is the thickness of the sample in cm, and I is the effective integral molar absorption coefficient in cm^{-1} mol^{-1} H l^{-1} (Paterson 1982). According to Paterson (1982), the value of I should be chosen according to the approximate level of OH concentration; a value of 24,000 cm^{-1} mol^{-1} H l^{-1} was taken for this study. Uncertainty associated with water contents is about 20–30%.

Table 1 Mineral proportions and oxygen isotope compositions of whole rocks and mineral separates from Tichka plutonic rocks

Sample	Rock type	Intrusion #	% quartz	% feldspar	% amphibole	% biotite	$\delta^{18}O$ whole rock	$\delta^{18}O$ biotite	$\delta^{18}O$ amphibole	$\delta^{18}O$ feldspar	$\delta^{18}O$ quartz	$\delta^{18}O$ muscovite
GOU6	Gabbro	2	0	47.8	14.3	4.5	5.9					
TAG154	Meladiorite	2	0	40	39.7	17.7	5.8	4.9				
TAG41	Diorite	3	4.7	54.4	23.8	14.3	7.3					
TAM28	Diorite	1	3.6	55.3	17	18.9	6.2	3.7	4.8	7.6	8.9	
TAG151	Diorite	2	1.1	66.4	14	13.5	6.5	2.8	5.1	7.1		
TAG110	Diorite	2	3.3	58.8	24.4	11.1	7.3	4.3	5.9	8.5		
TAG45	Diorite	3	2.1	58.3	20.9	16.5	7.9	4.9	5.1	8.9		
TAM29	Granodiorite	1	17	60.9	7.6	13.3	6.6	3.9	4.4	7.4	8.7	
TAG79	Granodiorite	2	12	61.9	9.8	12.3	6.8	4.5	5.1	7.6	9.0	
NFI19	Granodiorite	3	n.d	n.d	n.d	n.d	6.8					
GOU68	Granodiorite	2	n.d	n.d	n.d	n.d	6.9					
TAG105	Granodiorite	2	8.6	48.8	24.2	16.4	7.2					
NFI82	Granodiorite	3	17.9	66.3	9.3	5.4	8.1	3.1	4.6	8.4	8.7	
TAG126	Monzogranite	2	24.8	57.7	4.6	11.5	6.9	3.4	4.5	7.2	8.5	
TAG135	Monzogranite	2	29	60.4	2.4	7	7.1					
NFI72	Leucogranite	3	30.5	64.3	0	4.5	7.0	3.4		6.8	8.0	
ASF38	Leucogranite	4	n.d	n.d	n.d	n.d	8.7	5.9		8.7	8.8	
ASF39	Leucogranite	4	32.8	57.8	0	3.8	9.5					
NFI118	Leucogranite	4	n.d	n.d	n.d	n.d	10.4			10.0	8.9	6.1

Table 2 Distribution of mineral sizes for Tichka plutonic rocks

Sample	Rock type	Biotite (mm)	Muscovite (mm)	Amphibole (mm)	K-feldspar (mm)	Plagioclase (mm)	Quartz (mm)
TAG154	Meladiorite	0.1–0.7 (0.3)		0.1–0.8 (0.3)		0.1–2 (0.3)	
TAM28	Diorite	0.2–0.8 (0.4)		0.2–1.2 (0.6)		0.2–7 (1.5)	0.2–2 (0.6)
TAG110	Diorite	0.1–0.5 (0.3)		0.1–0.8 (0.3)		0.1–3 (0.6)	0.1–1 (0.2)
TAM29	Granodiorite	0.5–2 (1.2)		0.5–2 (1.2)		0.5–4 (2.5)	0.2–1.6 (0.4)
TAG79	Granodiorite	0.2–2 (1)		0.5–1 (0.8)	0.2–0.6 (0.4)	0.8–5 (1.5)	0.2–1.2 (0.6)
NFI82	Granodiorite	0.5–2 (0.8)		0.3–2 (1)	0.1–3 (1.5)	0.5–2 (1.5)	0.2–1 (0.8)
TAG126	Monzogranite	0.25–1 (0.8)		0.25–1.5 (0.8)	0.3–3 (2)	0.6–3 (2)	0.15–3 (1.5)
NFI72	Leucogranite	0.2–2 (1)			1–3 (2)	0.6–1.5 (1)	1–3 (1.5)
ASF38	Leucogranite	0.2–1 (0.8)			0.2–2 (0.8)	0.4–1.5 (0.8)	0.2–1.2 (0.8)
NFI118	Leucogranite	0.2	0.15–0.8 (0.5)		0.3–3 (1.5)	0.6–4 (1.2)	1–2.5 (1.5)

Bracketed values correspond to mean sizes

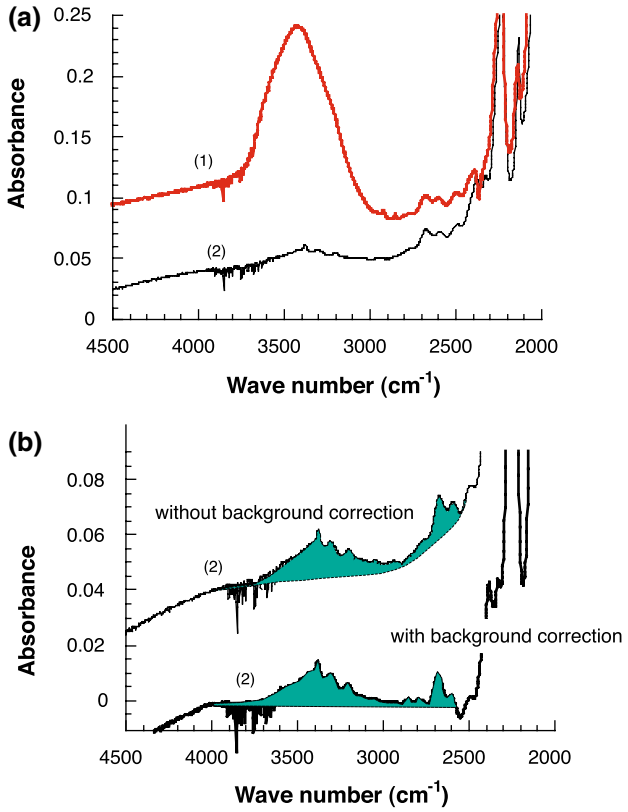

Fig. 3 **a** IR spectra of two quartz grains *1* and *2* from sample TAG126 showing the absorption band of the O–H species in the 2500–4000 cm^{-1} region. **b** Example of background correction for quartz grain *2*

Oxygen isotope data

Molecular oxygen, analyzed as CO_2 gas, was extracted at 600 °C during 12 h using the BrF_5 method (Clayton and Mayeda 1963). Isotopic compositions are quoted in the δ notation relative to VSMOW. Results from the NBS28 standard gave a mean $\delta^{18}O$ value of +9.5 ± 0.2‰. The external reproducibility of repeated measurements of Tichka whole rocks and mineral separates was better than 0.1‰ (2σ). Data are reported in Table 1.

Results

Transmission electronic microscopy

The microstructure of quartz from sample TAG126 is characterized by dislocations in climb configuration (Fig. 4). This configuration is indicative of plastic deformation at relatively high temperature (i.e. 450 °C) of water-containing quartz (Cordier et al. 1988; Cordier and Doukhan 1989). Higher temperature deformation (>450 °C) would be characterized by subgrain boundaries which are absent here. At lower temperature, or for dry quartz, climb of dislocation would not be allowed. It must also be mentioned that internal deformation of quartz crystals is also a function, besides temperature, of the planes to be activated, either parallel to the "c" axis (high *T*°, about 600 °C) or perpendicular to "c" (about 300 °C). Water-rich fluid inclusions are observed, either randomly distributed in the quartz matrix or along dislocations (Fig. 4), suggesting that the exsolution of this water took place before, during, and after the deforming event.

IR-spectroscopy

The calculated water contents are reported in Table 3 for fourteen spectra obtained from six quartz grains from sample TAG126 and range from 16.5 ppm H_2O (110 $H{\cdot}10^{-6}{\cdot}Si$) up to 373 ppm H_2O (2500 $H{\cdot}10^{-6}{\cdot}Si$), the highest values being measured in areas where fluid inclusions were clearly visible. Median and mean values of 35 ppm and 60 ppm

Table 3 Absorption for the O–H species measured between 2500 and 4000 cm^{-1} in quartz from monzogranite TAG126 (b and b2 in the analysis number corresponding to two different baselines subtracted to the spectrum)

Analysis number	Absorption (cm^{-2})	Thickness (cm)	Concentration (mol H/l)	Concentration ppm H_2O	Concentration $H \cdot 10^{-6}$ Si
060b	6.307	0.027	0.01	33.06	220.4
060b2	8.37	0.027	0.013	43.87	292.4
061b	6.92	0.029	0.011	36.27	241.8
061b2	6.15	0.029	0.009	32.23	214.9
062b	8.36	0.029	0.013	43.82	292.1
063b	60.3	0.029	0.093	316.04	2106.9
064b	17.76	0.029	0.027	93.08	620.5
065b	7.85	0.0277	0.012	41.14	274.3
066b	3.4	0.0277	0.005	17.82	118.8
066b2	3.47	0.0277	0.005	18.2	121.2
067b	29.24	0.0277	0.045	153.25	1021.7
068b	4.82	0.0262	0.007	25.26	168.4
069b	7.78	0.0262	0.012	40.78	271.8
070b	4.095	0.0262	0.006	21.46	143.1
071b	3.147	0.0229	0.005	16.5	109.9
072b	4.63	0.0229	0.007	24.27	161.8

Concentration of water is then calculated using the integral molar absorption coefficient given by Paterson (1982)

H_2O (400 $H \cdot 10^{-6} \cdot Si$) were respectively obtained for quartz from sample TAG126.

$\delta^{18}O$ of whole rocks

$\delta^{18}O$ values of Tichka whole rocks vary from 5.8 to 10.4‰ for a rock suite that spreads from gabbros to leucogranites. Except intrusion#4, the distribution of oxygen isotope compositions is not related to their belonging to the three other intrusive units (Table 1). Two samples from intrusion#1 have $\delta^{18}O$ values of 6.2 and 6.6‰. Oxygen isotope ratios of rocks from intrusion#2 vary from 5.8 to 7.3‰, whereas intrusion#3 is characterized by more positive $\delta^{18}O$ values (6.8–8.1‰). The highest $\delta^{18}O$ values (8.7–10.4‰) have been measured in the leucogranites of intrusion#4. Figure 5 shows variations in whole rock $\delta^{18}O$ values versus SiO_2 contents. We observe a rough increase of $\delta^{18}O$ values with SiO_2 contents, but the data distribution is complex and dependent on both the intrusion to which a given sample belongs and its petrology (Fig. 5). The lowest oxygen isotope compositions were measured in the gabbro (GOU6) and meladiorite (TAG154) of intrusion#2, whereas leucogranites from intrusion#4 constitute a separate cluster characterized by the highest $\delta^{18}O$ and SiO_2 values (Fig. 5). Excluding the case of intrusion#4, most of Tichka plutonic rocks have $\delta^{18}O$ values lower than 7.5‰ that slightly increase with the SiO_2 contents (see the linear trend illustrated in Fig. 5), except two samples belonging to intrusion#3 (TAG45 and NFI82). In more detail, diorites have a $\delta^{18}O$ range up to 2‰, a 1.5‰ difference occurs among granodiorites, and about 2‰ of isotopic variation affects leucogranites from intrusion#4.

$\delta^{18}O$ of minerals

Internal variations in $\delta^{18}O$ values of mineral separates (Table 1) reveal the narrow range of $\delta^{18}O$ values of quartz (from 8 to 9‰) in comparison to feldspar ($\delta^{18}O$ from 6.8 to 10‰), amphibole (from 4.4 to 5.9‰), and biotite (from 2.8 to 5.9‰). It is also remarkable that variations in the oxygen isotope compositions of quartz and amphibole are correlated to their modal abundance (Fig. 6) and mean grain size (Fig. 7). We emphasize that quartz grains were not systematically isolated from whole rocks for isotopic analysis because of either their absence in the primitive rocks or their minute abundance in some diorites (Table 1). The variation in $\delta^{18}O$ values of quartz (1‰) with respect to its modal abundance (Fig. 6a) is small relatively to the variation in whole rock $\delta^{18}O$ values (≈4‰). These correlations result from isotopic mass balance in a rock that behaves as a closed system, for example, when quartz crystallizes in abundance the remaining available ^{18}O reservoir is more diluted than for a rock in which minor amounts of quartz are formed at the end of the crystallization sequence. However, inverse trends have already been observed in other granite complexes (e.g., Tartèse and Boulvais 2010). The $\delta^{18}O$ values of whole rocks are mainly controlled by the $\delta^{18}O$ values of feldspar (Fig. 8a), which is the most abundant mineral present in Tichka plutonic rocks (Table 1). Consequently, this positive correlation (Fig. 8a) is not

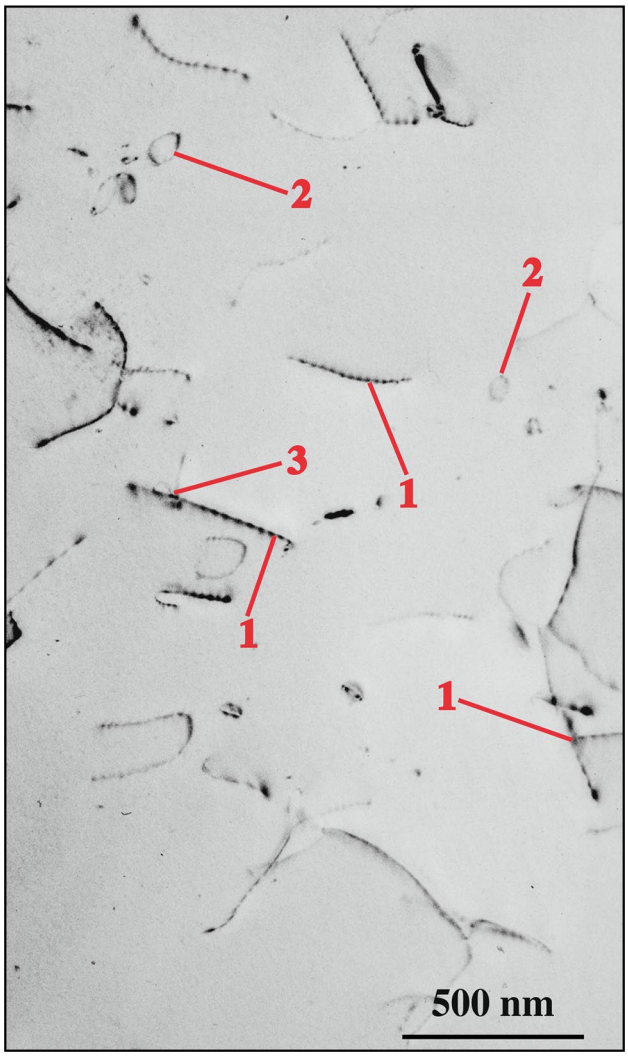

Fig. 4 Negative TEM image of a quartz grain showing numerous dislocations *1* in climb configuration. Tiny water bubbles *2* are also visible mostly dispersed in the quartz matrix, but also sometimes associated with the dislocations *3*

observed when variations in $\delta^{18}O$ values of quartz are reported against those of whole rocks (Fig. 8b). Considering the complex pattern of oxygen isotope compositions of Tichka plutonic rocks, we first explore whether the distribution of whole rock $\delta^{18}O$ values is totally related to their magmatic history or partly affected by a late hydrothermal or weathering stage.

Discussion

Post-solidus history of Tichka intrusions

The circulation of aqueous fluids during the sub-solidus history of plutons has the potential to modify the oxygen

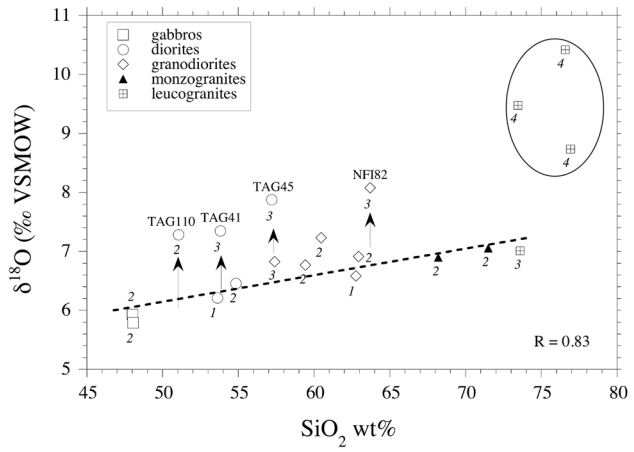

Fig. 5 Variations in whole rock $\delta^{18}O$ values versus SiO_2 contents. Alteration trends are materialized by *black arrows*. *Dashed line* linear correlation for the non-altered samples from intrusions #1 to #3 (TAG110, TAG41, TAG45, and NFI82 are excluded from this trend). The open field delimits the samples from intrusion#4. *Symbol size* represents the analytical uncertainty associated with the repeated measurements of whole rock $\delta^{18}O$ values

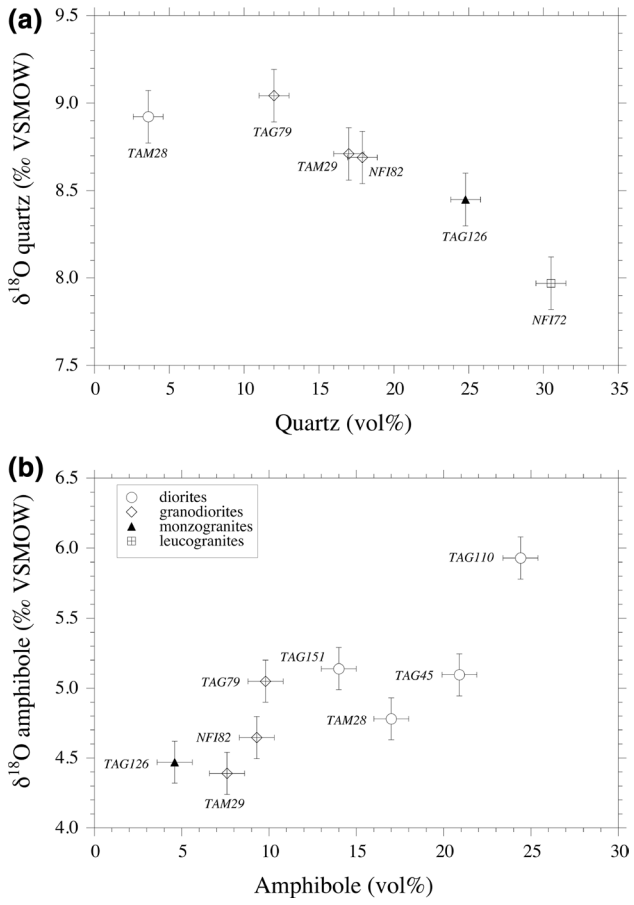

Fig. 6 Variations in $\delta^{18}O$ values of quartz (**a**) and amphibole (**b**) as a function of their modal abundance (% volume). Same symbols as in Fig. 5

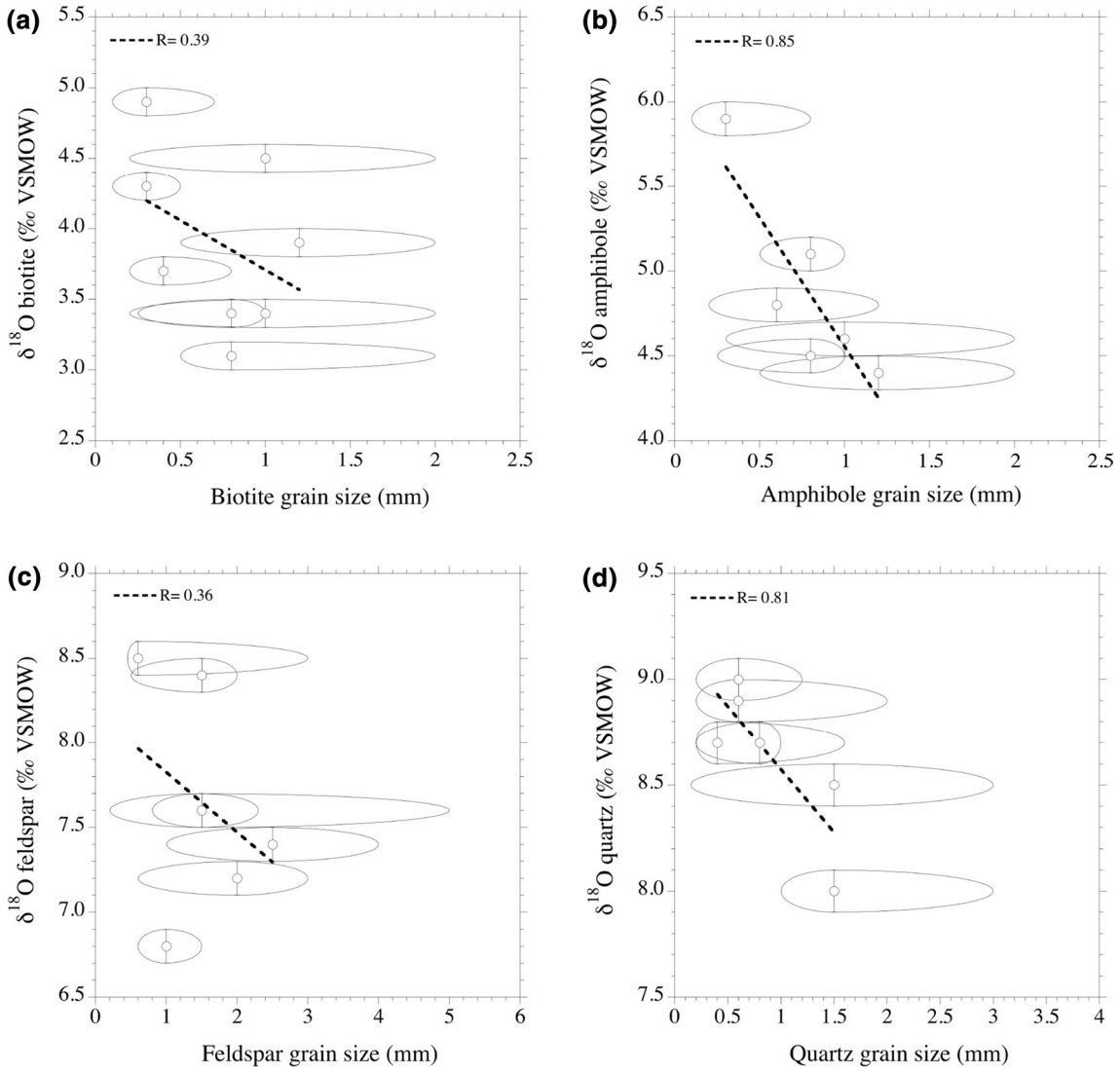

Fig. 7 Variations in $\delta^{18}O$ values of biotite (**a**), amphibole (**b**), feldspar (**c**), and quartz (**d**) as a function of their mean grain size

isotope compositions of cooling rocks (e.g., Taylor 1978). First, it is critical to examine the possible existence of isotopic heterogeneities related to a weathering or hydrothermal stage before modeling cooling rates and discussing any process of crustal contamination. An apparent complexity in the distribution of $\delta^{18}O$ values of Tichka rocks is well illustrated when reported against SiO_2 contents (Fig. 5) or the initial Sr and Nd isotope compositions (Fig. 9).

The examination of apparent oxygen isotope fractionations, between the mineral pairs that constitute the whole rocks, may reveal disequilibrium patterns, which are characteristics of water–rock interactions (Gregory et al. 1989). When the $\delta^{18}O$ values of feldspars are plotted against those of quartz (Fig. 10a), we observe that a series of five rocks (NFI72, TAG126, TAM29, TAM28, and TAG79) plot along a line that corresponds to a Δquartz-feldspar of +1.3. This fractionation value is in agreement with an undisturbed sub-solidus magmatic evolution where quartz and feldspar stopped exchanging oxygen isotopes during cooling at a temperature of about 600 °C according to the isotopic fractionation equations developed by Bottinga and Javoy (1975). We note, however, that three samples exhibit typical disequilibrium isotopic patterns with Δquartz-feldspar close to 0 or even negative (Fig. 10a). Similar closure isotopic temperatures of 580 ± 20 °C are obtained from amphibole-quartz pairs (Fig. 10b) except for samples TAM28 and TAM29 that show higher Δquartz-amphibole values. These higher fractionation values could mean lower closure isotopic temperatures; however, the amphiboles from these two samples are Fe-hornblende instead of Mg-hornblende. (Kohn and Valley 1998) have shown that Mg–Fe substitutions in amphiboles are able to modify by several tenths of

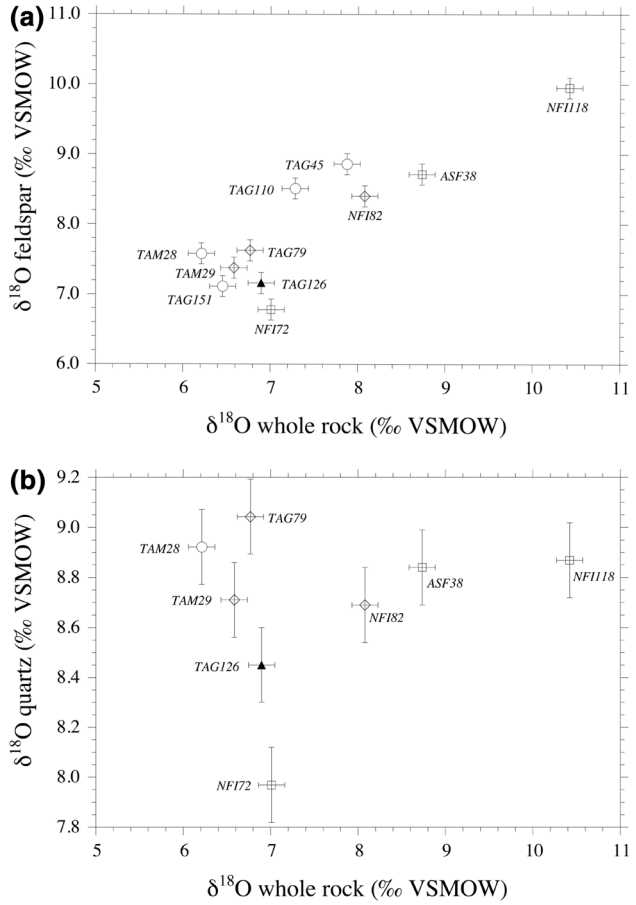

Fig. 8 Variations in $\delta^{18}O$ values of feldspar (**a**) and quartz (**b**) as a function of whole rock $\delta^{18}O$ values. Same symbols as in Fig. 5

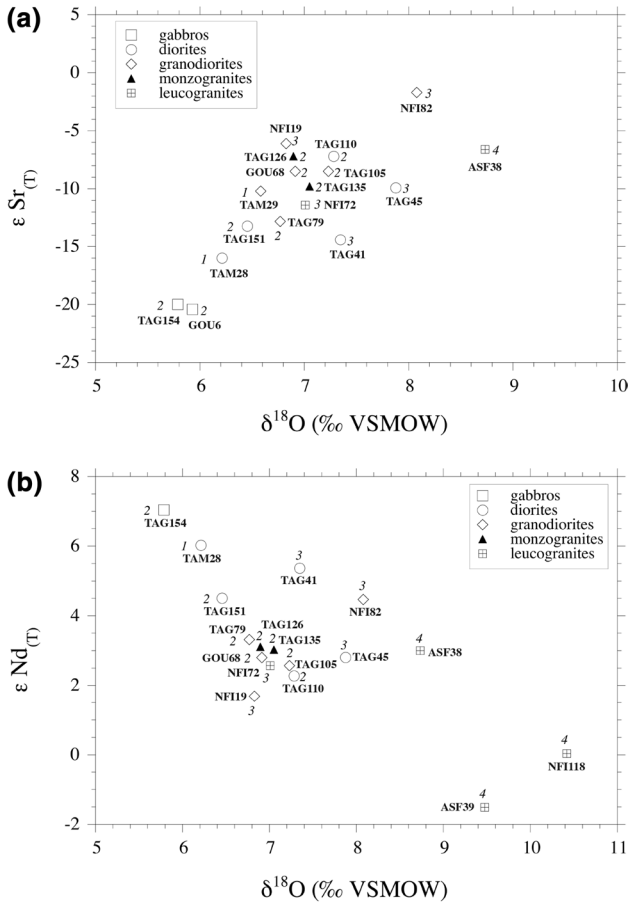

Fig. 9 Variations in εSr(T) (**a**) and εNd(T) (**b**) values as a function of whole rock $\delta^{18}O$ values. Sr and Nd isotope data are from Gasquet et al. (1992). Same symbols as in Fig. 5

per mil the oxygen isotope fractionation between mineral and water. Unfortunately, as already noted, it was not possible to analyze systematically the quartz–feldspar pairs. If we examine the other samples with high $\delta^{18}O$ values, we can suspect some of them to have also been hydrothermally altered. Sample TAG45 from intrusion#3 is characterized by Δfeldspar–amphibole and Δamphibole–biotite values compatible with isotopic disequilibria in the presence of an aqueous fluid phase (Table 1). Sample TAG41 very close to TAG45 (Fig. 1) remains questionable in the absence of mineral $\delta^{18}O$ values, whereas sample TAG110 has recorded fractionations for feldspar–amphibole ($\Delta = 2.6$) and feldspar–biotite ($\Delta = 4.2$) pairs, compatible with a magmatic history.

Δfeldspar–quartz values that range from 0 to 1 for samples (samples NFI118, NFI82, and ASF38) reveal disequilibrium processes that are not related to a simple magmatic history (Criss and Taylor 1986; Criss et al. 1987; Gregory et al. 1989). On the basis of our data, only feldspars from samples NFI118, NFI82, and ASF38 have oxygen isotope compositions that strongly deviate from apparent isotopic equilibrium temperatures (Criss and Taylor 1986). It is also worth noting that the two-mica leucogranites (NFI118 and ASF38), with high whole rock $\delta^{18}O$ values, were hydrothermally altered, strongly contrasting with the leucogranite NFI72 from intrusion#3 whose belongs to the general trend drawn by most of the samples (Fig. 5). If samples for which the oxygen isotope compositions have been modified by water–rock interactions are not considered anymore, smooth regular trends of $\delta^{18}O$ values increasing by 1.5‰ for large variations in SiO_2 contents (see trend in Fig. 5) and the initial Sr isotope compositions (Fig. 9a) are then observed.

We, therefore, conclude that the original oxygen isotope compositions of some plutonic rocks (TAG45, NFI82, ASF38, NFI118, and TAG41?) from the TPC were modified through sub-solidus alteration by an aqueous fluid. Feldspars were ^{18}O-enriched during a low-temperature stage of water–rock interaction (Fig. 10a), a pattern of isotopic exchange which strongly contrasts with those well known during the hydrothermal alteration of

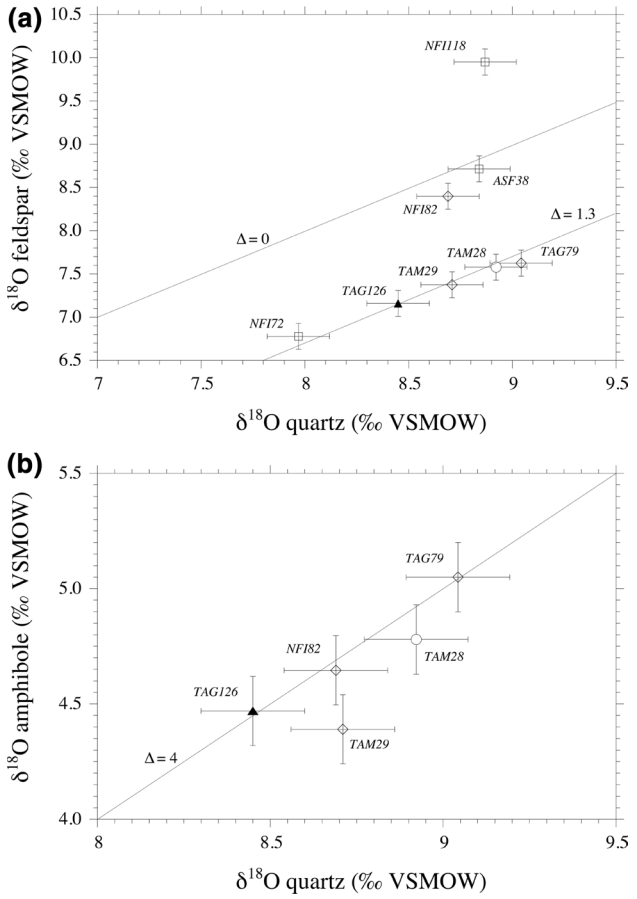

Fig. 10 $\delta^{18}O$ of feldspar (**a**) and amphibole (**b**) versus $\delta^{18}O$ of quartz from some Tichka plutonic rocks. *Full lines* represent isotherms computed with fractionation values of mineral pairs according to equations of Bottinga and Javoy (1975). **a** Five mineral pairs have fractionations of about +1.3 that indicate apparent temperatures of about 600 °C, whereas three others (NFI82, NFI118, and ASF38) show isotopic disequilibrium produced by a late low-temperature hydrothermal circulation that enriched feldspars in ^{18}O relatively to quartz. **b** Three mineral pairs have a fractionation value of +4 ($T = 580$ °C), whereas the two other samples (TAM28 and TAM29) show apparent lower temperatures. Same symbols as in Fig. 5

continental plutons by meteoric waters (e.g. Taylor 1977). As it was commonly demonstrated, because of the ubiquitous ^{18}O-depleted character of meteoric waters, interaction of such waters with igneous rocks at temperatures higher than 200–300 °C generate low $\delta^{18}O$ hydrothermally altered igneous rocks (Taylor 1977; Taylor and Sheppard 1986). An ^{18}O-enrichment of igneous rocks may be produced at lower temperatures as already documented during weathering (Lawrence and Taylor 1971) and also in the surficial zones of certain hydrothermal systems (Criss et al. 1984). These isotopic patterns mainly result from the property of the oxygen isotope fractionation equation between feldspar and water; at temperatures of water–rock interactions higher than 250 °C, feldspars are ^{18}O-depleted relatively to their magmatic values, while they become ^{18}O-enriched at low temperatures. Such reversed temperature-dependent oxygen isotope fractionation has also been documented in the hydrothermally altered oceanic crust (Gregory and Taylor 1981; Lécuyer and Fourcade 1991; Lécuyer and Reynard 1996). We cannot also exclude that aqueous fluids with positive $\delta^{18}O$ values could have been released during the heating of intruded pelites or metabasites. Such a hypothesis was already proposed as a source of aqueous fluids that interacted with the Variscan granites from the Pyrénées (Fourcade and Allègre 1981).

Except along the margins of the Tichka plutonic complex, the hydrothermal activity was rather limited, perhaps, as the consequence of the low permeability of country rocks mainly made of pelites and metabasites. Taking into account this limited hydrothermal activity, the rates at which these intrusions cooled must be investigated.

Cooling rates of Tichka plutons

Modeling cooling rates with oxygen isotope data

The distribution of $\delta^{18}O$ mineral values constituting an igneous rock, which has cooled in a closed system, depends on (1) the cooling rate, (2) the mineral grain sizes, and (3) the proportions of minerals in the rock (Giletti 1986; Eiler et al. 1992, 1993). Using the kinetic data for oxygen self-diffusion in quartz, feldspar, hornblende, and biotite, which are the four dominant minerals present in the Tichka plutonic rocks, cooling rates can be calculated for rocks that escaped hydrothermal alteration and for which modal data (Table 1) and mineral sizes are available (Table 2). A similar approach has been made by Durand et al. (2006; see Fig. 7) who modeled oxygen isotope profiles in the Quérigut magmatic complex, Eastern Pyrenees, France. Cooling rates were calculated (Table 4) on the basis of the best fit between calculated by mass balance and measured $\delta^{18}O$ values of minerals following the procedure developed by Giletti (1986) which involves Dodson's (1973) Eq. (2);

$$T_c = \frac{\frac{E}{R}}{\ln\left[\frac{-ART_c^2\left(\frac{D_O}{a^2}\right)}{E\left(\frac{dT}{dt}\right)}\right]} \quad (2)$$

in combination with the mass–balance relationship (3);

$$\delta^{18}O_{(\text{whole rock})} = \left[\sum_{i=1}^{n} X_j(\delta^{18}O_i - \Delta_{ij})\right] + X_i\delta^{18}O_i \quad (3)$$

where T_c is the closure temperature of isotope exchange, E is the activation energy for self-diffusion of oxygen in a given mineral, A is the diffusional anisotropy parameter, R is the gas constant, D_o is the pre-exponential factor, a is the

Table 4 Estimates of cooling rates based on the best fit between measured and modeled $\delta^{18}O$ minerals and whole rocks

	$\delta^{18}O$ analyzed	$\delta^{18}O$ modeled	Mineral pairs	Apparent T °C
TAM28 (pluton#1)				
Whole rock	6.2	6.0	qtz-amp	573
Quartz	8.9	9.0	qtz-feld	591
Amphibole	4.8	4.5	qtz-biot	525
Feldspar	7.6	7.3	amp-feld	566
Biotite	3.7	3.5	amp-biot	348
			feld-biot	504
Cooling rate = 10–50 °C My^{-1}				
TAM29 (pluton#1)				
Whole rock	6.6	6.8	qtz-amp	555
Quartz	8.7	8.9	qtz-feld	591
Amphibole	4.4	4.9	qtz-biot	554
Feldspar	7.4	7.2	amp-feld	540
Biotite	3.9	3.9	amp-biot	549
			feld-biot	542
Cooling rate = 10–50 °C My^{-1}				
TAG79 (pluton#2)				
Whole rock	6.8	6.9	qtz-amp	593
Quartz	9.0	9.0	qtz-feld	559
Amphibole	5.1	5.0	qtz-biot	578
Feldspar	7.6	7.4	amp-feld	609
Biotite	4.5	4.3	amp-biot	502
			feld-biot	584
Cooling rate = 10–50 °C My^{-1}				
TAG126 (pluton#2)				
Whole rock	6.9	6.8	qtz-amp	583
Quartz	8.5	8.4	qtz-feld	591
Amphibole	4.5	4.6	qtz-biot	532
Feldspar	7.2	7.0	amp-feld	579
Biotite	3.4	3.2	amp-biot	348
			feld-biot	513
Cooling rate = 10–50 °C My^{-1}				
NFI72 (pluton#3)				
Whole rock	7.0	6.9	qtz-amp	–
Quartz	8.0	7.9	qtz-feld	626
Amphibole	–	–	qtz-biot	569
Feldspar	6.8	6.7	amp-feld	–
Biotite	3.4	3.4	amp-biot	–
			feld-biot	552
Cooling rate = 500–1000 °C My^{-1}				

These calculations were made assuming dry minerals and oxygen isotope diffusion in a closed system. Resulting apparent isotopic temperatures are also reported for each possible mineral pair. Fractionation factors are derived from equations given by Bottinga and Javoy (1975). Oxygen diffusion data come from Giletti and Anderson (1975) and Giletti (1986). Uncertainties associated with calculated temperatures are about ±30 °C

mineral size, dT/dt is the cooling rate, X is the modal abundance of minerals i, j, and Δ is the fractionation factor for mineral pairs. References for oxygen diffusion and isotopic fractionation data are given along with the Table 4.

Five samples were selected to calculate the cooling rates of intrusions #1, #2, and #3. Large differences among computed apparent temperatures for mineral pairs reflect low cooling rates. Calculations lead to a cooling rate of 10–50 °C My^{-1} for intrusion #1 and #2 and a much higher

estimate for intrusion#3 of 500–1000 °C My^{-1}. One interesting effect of cooling rate is the isotopic mass balance effect at the whole rock scale resulting from the various proportions of minerals and the time at which isotopic diffusion for each mineral stopped. This mass balance effect is recorded in the various minerals and we observe that their variations in $\delta^{18}O$ values against SiO_2 contents do not resemble variations in $\delta^{18}O$ values of whole rocks (Fig. 5). Figure 6 shows that $\delta^{18}O$ values of quartz decrease with increasing modal abundance of quartz (and also magmatic differentiation), whereas $\delta^{18}O$ of amphiboles increase with the amount of these amphiboles in the rocks. Another expected consequence of the cooling rate of these rocks is some dependence observed between the $\delta^{18}O$ values of minerals and their mean grain size (Fig. 7).

Cooling rates of about 10–50 °C My^{-1} for intrusions #1 and #2 may be considered as surprisingly very low cooling rates for intrusions whose diameters do not exceed 10 km (Fig. 1) and whose emplacement depths range from 4 to 6 km. Indeed, we would expect in such plutonic suite that the cooling rate should decrease from the first to the latest intrusion because of the heat advected by the successive magma injections. The pluton was supposed built by ballooning (Lagarde and Roddaz 1983) and to be the result of in-situ assemblage of four magma batches (Gasquet 1991) which were injected into pre-existing country rocks in relation to transpressional tectonic regime as well demonstrated in similar plutonic complexes (Wang et al. 2002; Asrat et al. 2003; Glazner et al. 2004; Matzel et al. 2006; Barbey et al. 2008; Clemens et al. 2009). However, according to recent works performed by Annen et al. (2015), Menand (2011), Menand et al. (2015), and Coleman et al. (2016), the four magmatic bodies of the TPC may result from the amalgamation of magmatic dykes injected rapidly and successively. Giletti (1986) calculated a cooling rate in the range 100–200 °C My^{-1} for the San Jose tonalite and Hess et al. (1993) a cooling rate of 180 °C My^{-1} for the Eldzhurtinskiy granite (Caucasus) whose sizes are comparable to the TPC. Such low cooling rates for intrusions #1 and #2 could result from the very limited or near absent hydrothermal activity which is well known to be a very efficient process to remove heat from the crust. Each new intrusion could also heat the previous one, thus lowering its cooling rate. It must be noted that a much higher cooling rate of 500–1000 °C My^{-1} was computed for the intrusion#3. Even though this intrusion shows more evidence of hydrothermal circulation at the field scale (Gasquet 1991), sample NFI72 most likely preserved a magmatic oxygen isotope composition as suggested by its Δquartz-feldspath value of +1.3 (Fig. 10a). It must be noted that the whole rock modeling is less constrained than for other samples with only three minerals in the absence of amphibole (Table 4). Therefore, we do not consider this estimated high cooling rate as meaningful. Computed slow cooling rates of 10–50 °C My^{-1} may also be explained either by a protracted magmatic history within each pluton or by the imbricated structure of these plutons for which the new intrusion heated the former one, thus lowering its cooling rate overall. All these calculated cooling rates inferred from an isotopic modeling based on data of self-diffusion of oxygen in minerals must be compared to a simple model of thermal cooling of a pluton whose size and emplacement depth are similar to those occurring in the Tichka plutonic complex.

Constraints from thermal modeling of a single pluton

The following 2D thermal balance equation which takes into account the latent heat of fusion and crystallization (Stüwe 1995) has been solved by a finite-difference method using an ADI scheme (Albarède 1995):

$$c_p \frac{\partial T}{\partial t} + L\frac{\partial v}{\partial t} = \left(\frac{k}{\rho}\right)\left(\frac{\partial^2 T}{\partial x^2} + \frac{\partial^2 T}{\partial y^2}\right) + \left(\frac{A}{\rho}\right) \quad (4)$$

with T being the temperature, ρ the density, t time, k thermal conductivity, A radiogenic heat production, v melt proportion, L latent heat of fusion, and c_p the heat capacity. The values of the parameters are given in Table 5. The term concerning the fusion is solved by the method of Price and Slack (1954) who proposed to use a modified heat capacity equal to:

$$c_{\mathrm{mod}} = c_p + L\frac{\partial v}{\partial t}. \quad (5)$$

In the melting interval, an exponential model of melt proportion according to temperature has been used (Stüwe 1995):

$$\frac{\partial v}{\partial T} = Be^{\alpha T}. \quad (6)$$

Table 5 Physical parameters used in the thermal model

ρ	Density	2700 kg m^{-3}
c_p	Heat capacity	1000 J kg^{-1} K^{-1}
c_{mod}	Modified heat capacity	
L	Latent heat of crystallization	320×10^3 J kg^{-1}
v	Proportion of melt	
Ts	Solidus temperature	700 °C
Tl	Liquidus temperature	900 °C
K	Thermal conductivity	2.5 W m^{-1} K^{-1}
A	Radiogenic heat production	1 μW m^{-3}
α	Exponential parameter in Eq. 6	0.001 K^{-1}
B	Pre-exponential parameter in Eq. 6	0.0022 K^{-1}

See Table 5 for the description of the parameters. The evolution of melt proportion with temperature is not a key parameter in this model as it is concerned by the temperature evolution after the crystallization phase. The values of B and α are, therefore, not important in the model as they describe the shape of the fusion curve. The liquidus and solidus temperatures and the latent heat (Table 5) used in calculation are those of a granitic magma (Stüwe 1995).

The initial and boundary conditions of the system are described in Fig. 11. The calculation domain is 20 km long and 15 km thick. It is assumed that the emplacement of the intrusion, is rapid on the right mirror boundary of the domain at 5 km depth. It means that this thermal modeling of a single isolated pluton only provides an estimate of the upper limit for the cooling rate. The thickness of melted body is 4 km and its width is 5 km. The initial undisturbed geotherm is a simple parabolic one (Turcotte and Schubert 1982) with a surface temperature of 0 °C, an internal heat production of 1 μ W m^{-3}, and a basal heat flow of 37 m W m^{-2}. The surface and the left boundaries of the model have constant temperatures. The heat flow is constant at the base of the system and nul on the right boundary.

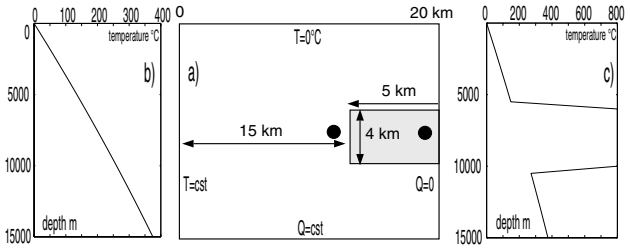

Fig. 11 **a** Geometry and boundary conditions of the thermal model. The *box* represents the intrusion. The *points* indicate the areas on which the temperature evolution has been measured. **b, c** Initial geotherms on the left and right boundaries of the model. *Cst* constant

The temperature evolution of two points has been followed (Fig. 12), one in the middle of the intrusion, the other at 7.5 km depth in the country rocks, 3 km off the intrusion boundary. One hundred thousand years after the emplacement, cooling rate in the intrusion reaches 1900 °C My^{-1} at 600 °C and is between 10 and 50 °C My^{-1} after 0.45 My when the intrusion temperature is around 380 °C. We note that these values are the lowest possible as the effect of convection in the intrusion and in the fluids in the surrounding rocks are not taken into account. The cooling rates estimated by the thermal model are then two orders of magnitude higher than those estimated from the distribution of δ^{18}O mineral values for the intrusion #1 and #2 (Table 4). A re-examination of the parameters of the geochemical model has been done to explain this discrepancy.

The incorporation of water into quartz and its role on oxygen diffusion

It is well known and this has been particularly well studied in quartz (e.g., Cordier and Doukhan 1989), that the incorporation of even small amounts of water modifies the

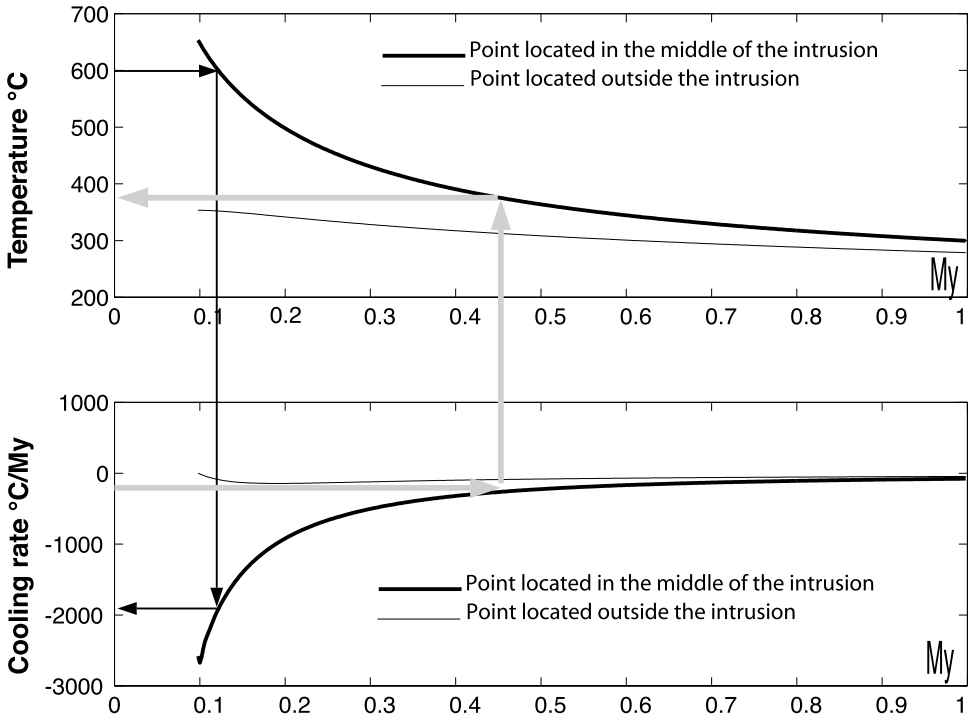

Fig. 12 **a** Temperature evolution of the areas marked by points on Fig. 11a. **b** Cooling rates of the same points. At 600 °C in the intrusion, the cooling rate is 1900 °C My^{-1}. A value of 10–50 °C My^{-1} is reached after 0.45 My when the temperature in the intrusion is close to the steady-state temperature of the system

physical and chemical properties of quartz, such as ductility and diffusivity. Infrared spectroscopy (IR) was, therefore, used to quantify the amount of water dissolved in these quartz grains.

The solubility of water in quartz has been shown experimentally and theoretically to be extremely low, even at high pressure. It is in the order of few tens of $H{\cdot}10^{-6}$ Si, reaching 50 to 100 $H{\cdot}10^{-6}$ Si at 700 °C and 800 MPa (Cordier and Doukhan 1989). In natural as well as in synthetic crystals; however, it is common to find larger amounts of water (up to few thousands $H{\cdot}10^{-6}$ Si), showing that under specific conditions (large water fugacities, rapid growth) supersaturated water can be incorporated into the quartz structure. Several models exist for the incorporation of water into the quartz structure (e.g., Paterson 1986; McConnell 1995). For a small concentration of water, it can be dissolved under the form of point defects [the (4 H) Si defects where 1 Si is replaced by 4 H] or under the form of tiny fluid inclusions. For a large amount of water (i.e., when supersaturated H_2O is present), it is then essentially under the form of tiny fluid inclusions as occurring in the sample investigated in this study (Fig. 4).

Both microstuctures such as dislocations in climb configuration, tiny bubbles (Cordier and Doukhan 1989), as well as water content determinations (average value around 400 $H{\cdot}10^{-6}$ Si) suggest that quartz grains in the selected TAG126 sample contain large amounts of supersaturated water and can be considered as wet quartz crystals. Such observation allows reconsidering the rate of oxygen diffusion, since it is well known that water enhances the rates of many solid-state diffusional processes. For instance, it has been shown that diffusion coefficients for oxygen in quartz are markedly greater in hydrothermal experiments (e.g. Giletti and Yund 1984) than those measured under anhydrous conditions (e.g., Schactner and Sockel 1977). Moreover, by comparing the diffusion law for water in wet quartz described by Cordier et al. (1988) with experimentally determined diffusion coefficient for oxygen in quartz under hydrothermal conditions (Dennis 1984; Giletti and Yund 1984; Farver and Yund 1991), it appears that the oxygen diffusion process is certainly controlled by the diffusion of molecular water in quartz as already suggested by several authors (Farver and Yund 1991; McConnell 1995). To model the oxygen diffusion in the quartz grains of the Tichka intrusion, we have used, according to Cordier et al. (1988), the following water diffusion law (7):

$$D = 10^{-12} \exp\left(\frac{-95,000}{RT}\right) \mathrm{m^2 s^{-1}}. \quad (7)$$

In these wet conditions, a numerical application shows that D is at least an order of magnitude higher than those experimentally determined for oxygen-self-diffusion in dry quartz. True cooling rates are, therefore, expected to be in the range 500–1000 °C My^{-1}, which are in better agreement with the results deduced from the thermal modeling of a single pluton. Such fast cooling rates could explain why during assimilation of the various country rocks, heterogeneities of the neodymium and strontium isotope ratios were preserved (Fig. 9).

Crustal contamination

Excluding isotopically altered samples (TAG110, TAG41, TAG45 and NFI82), a decrease in the scattering of $\delta^{18}O$ values with respect to SiO_2 contents and a good correlation with the initial Sr isotope ratios are observed (Figs. 5, 9). There is, indeed, no more than 0.5‰ of variation in $\delta^{18}O$ values for identical Sr isotope compositions. Leucogranites from intrusion#4 constitute a separate group of rocks (Fig. 5). Gasquet et al. (1992) have shown that these leucogranites are not related to the other intrusions and were generated by melting of a supracrustal source. Their low $\delta^{18}O$ values for S–type granites (Taylor 1978) reveal the ^{18}O-depleted character of the Paleozoic wall-rocks compared to modern sediments.

The dioritic–monzogranitic suite of the TPC was generated through a combined process of crystallization and assimilation of country rocks as it was demonstrated by Gasquet et al. (1992). The most peculiar isotopic feature of these plutonic rocks is the slight $\delta^{18}O$ increase, which does not excess 1–1.5‰ (Fig. 5), recorded by the most evolved terms (monzogranites and biotite–leucogranites) of intrusions#2 and #3. Unmetamorphosed sediments are generally characterized by much higher $\delta^{18}O$ values, typically in the range 15–25‰ (Taylor 1978). When they are involved into crustal contamination of a mantle source, the igneous products have generally higher $\delta^{18}O$ values than those observed for Tichka plutonic rocks ($\delta^{18}O$ = 6–7.5‰) as it is the case for the contemporaneous Variscan Pyrénées ($\delta^{18}O$ = 10–12‰; Wickham and Taylor 1985, 1987) or Corsican ($\delta^{18}O$ = 6–9‰; Cocherie et al. 1994) calc-alkaline granitoids. Published Sr and Nd isotope data revealed that the mechanism of magma genesis for the TPC implied a moderate rate (no more than 30%) of crustal component recycling (Gasquet et al. 1992). According to this result, the oxygen isotope compositions of Tichka plutonic rocks suggest that the crustal components (metamorphosed pelitic and volcanic rocks) involved in the crustal contamination of the mantle source had $\delta^{18}O$ values lower than 10‰. It has been indeed documented through several studies that Paleozoic wall-rocks tend to have lower $\delta^{18}O$ values than modern ones (Simon and Lécuyer 2005 and references therein). In the absence of these Sr or Nd isotope data, it would be highly speculative to interpret these data, because a

$\delta^{18}O$ increase of 1–1.5‰ from mafic to felsic rocks may be expected for a simple fractional crystallization history (Weiss et al. 1987).

Compared with the West European Variscan plutons, the Moroccan TPC is quite similar to the post-collisional granitoids from the Northern Armorican Massif, Northeastern French Central Massif, Northern Vosges, or Northwestern Portugal (see references in Gasquet et al. 1996; Dias et al. 2002; Simons et al. 2016). However, contrary to this European segment where the post-collisional granitoids are generally associated with late extensional tectonics and shear-zones, the emplacement of the Tichka would be mainly controlled by transpressive tectonics partly comparable to the post-closure tectonics of Pitcher (1983). The crustal magma genesis implies, in both Variscan segments, significant thermal anomalies related to the emplacement of mantle-derived magmas inducing crustal anatexis (e.g., Vielzeuf and Pin 1989).

Concluding remarks

By combining results from thermal modeling of a single pluton both, knowledge of self-oxygen diffusion data of rock-forming minerals and the determination by IR-spectroscopy of the water content of quartz, the cooling rates of Tichka plutons have been estimated in the range 500–1000 °C My^{-1}, which corresponds to a cooling duration from 10^5 to 5×10^5 years. Such conclusions match those inferred from $^{40}Ar/^{39}Ar$ ages obtained for the Hercynian Lizio granite of quite similar size. Indeed, Tartèse et al. (2011) estimated that the Lizio granite cooled down in less than one million of years. Such high cooling rates calculated for the Tichka plutons are also in agreement with the small sizes of individual intrusions (diameter <10 km) and their shallow depth of emplacement between 4 and 6 km. The rapid cooling of the intrusions may explain why during assimilation of the various country rocks, heterogeneities of the neodymium and strontium isotope ratios were preserved. These cooling rates are consistent with geochronological data and the previous models obtained for pluton assembly for recently studied similar intrusions (St Jean du Doigt massif, Barboni et al. 2013, 2015; Mt Capanne pluton). The combination of O, Sr, and Nd isotope data suggests that during the magma ascent towards the surface, no more than 30% of metapelites or metabasites were assimilated. These metasediments are most likely characterized by $\delta^{18}O$ values lower than 10‰. Finally, a late stage of limited hydrothermal activity affected some plutonic rocks whose fluid source could have derived from the dehydration of the Paleozoic basement during the emplacement of the Tichka plutonic complex.

Acknowledgements The authors warmly thank Ph. Boulvais and M. de Saint Blanquat for their reviews that significantly improved the scientific content of this study.

References

Albarède F (1995) Introduction to geochemical modeling. University Press, Cambridge, p 554

Annen C, Blundy JD, Sparks RSJ (2006) The genesis of intermediate and silicic magmas in deep crustal hot zones. J Petrol 47:505–539

Annen C, Blundy JD, Leuthold J, Sparks RSJ (2015) Construction and evolution of igneous bodies: Towards an integrated perspective of crustal magmatism. Lithos 230:206–221

Asrat A, Gleizes G, Barbey P, Ayalew D (2003) Magma emplacement and mafic-felsic magma hybridization: structural evidence from the Pan-African Negash pluton, Northern Ethiopia. J Struct Geol 25:1451–1469

Ballouard C, Boulvais P, Poujol M, Gapais D, Yamato P, Tartèse R, Cuney M (2015) Tectonic record, magmatic history and hydrothermal alteration in the Hercynian Guérande leucogranite, Armorican Massif, France. Lithos 220–223:1–22

Bando M, Bignall G, Sekine K, Tsuchiya N (2003) Petrography and uplift history of the Quaternary Takidani Granodiorite: could it have hosted a supercritical (HDR) geothermal reservoir? J Volcanol Geotherm Res 120:215–234

Barbey P, Gasquet D, Pin C, Bourgeix AL (2008) Igneous banding, schlieren and mafic enclaves in calc-alkaline granites: the Budduso pluton (Sardinia). Lithos 104:147–163

Barboni M, Schoene B, Ovtcharova M, Bussy F, Schaltegger U, Gerdes A (2013) Timing of incremental pluton construction and magmatic activity in a back-arc setting revealed by ID-TIMS U/Pb and Hf isotopes on complex zircon grains. Chem Geol 342:76–93

Barboni M, Annen C, Schoene B (2015) Evaluating the construction and evolution of upper crustal magma reservoirs with coupled U/Pb zircon geochronology and thermal modeling: a case study from the Mt. Capanne pluton (Elba, Italy). Earth Planet Sci Lett 432:436–448

Bottinga Y, Javoy M (1975) Oxygen isotope partitioning among the minerals in igneous and metamorphic rocks. Rev Geophys 13:401–418

Chappell BW (2004) Towards a unified model for granite genesis. Trans R Soc Edinb Earth Sci 95:1–10

Christofides G, Perugini D, Koroneos A, Soldatos T, Poli G, Eleftheriadis G, Del Moro A, Neiva AM (2007) Interplay between geochemistry and magma dynamics during magma interaction: an example from the Sithonia Plutonic Complex (NE Greece). Lithos 95:243–266

Clayton RN, Mayeda TK (1963) The use of bromine pentafluoride in the extraction of oxygen from oxides and silicates for isotopic analyses. Geochim Cosmochim Acta 27:43–52

Clemens JD, Helps PA, Stevens G (2009) Chemical structure in granitic magmas – a signal from the source? Trans R Soc Edinb Earth Sci 100:159–172

Cocherie A, Rossi P, Fouillac AM, Vidal P (1994) Crust and mantle contributions to granite genesis—an example from the Variscan batholith of Corsica France, studied by trace-element and Nd-Sr-O-isotope systematics. Chem Geol 115:173–211

Coleman DS, Mills RD, Zimmerer MJ (2016). The pace of plutonism. Elements 12:97–102.

Collins WJ, Richards SR, Healy BE, Ellison PI (2000) Origin of heterogeneous mafic enclaves by two-stage hybridisation in magma

conduits (dykes) below and in granitic magma chambers. Trans R Soc Edinb Earth Sci 91:27–45
Cordier P, Doukhan JC (1989) Water solubility in quartz and its influence on ductility. Eur J Mineral 1:221–237
Cordier P, Boulogne B, Doukhan JC (1988) Water precipitation and diffusion in wet quartz and wet berlinite $AlPO_4$. Bull Minéral 111:113–117.
Creaser RA (1996) Petrogenesis of mesoproterozoic quartz latite-granitoid suite from the Roxby Downs area, South Australia. Precamb Res 79:371–394.
Criss RE, Taylor HP (1986) Meteoric-hydrothermal systems. In: Valley JW, Taylor HP Jr, O'Neil JR (eds) Stable isotopes in high temperature geological processes, vol 16. Mineral Society of America, Washington, DC, pp 373–424
Criss RE, Ekren EB, Hardyman RF (1984) Casto ring zone: a 4,500 km^2 fossil hydrothermal system in the Challis volcanic field, central Idaho. Geology 12:331–334
Criss RE, Gregory RT, Taylor HPJr (1987) Kinetic theory of oxygen isotopic exchange between minerals and water. Geochim Cosmochim Acta 51:1099–1108
De Paolo DJ (1981) Trace element and isotopic effects of combined wallrock assimilation and fractional crystallization. Earth Planet Sci Lett 53:189–202
Dennis PF (1984) Oxygen self-diffusion in quartz under hydrothermal conditions. J Geophys Res 89:4047–4057
Dias G, Simoes PP, Ferreiera N, Leterrier J (2002) Mantle and crustal sources in the genesis of t lmate hercynian hybrid granitoids (NW Portugal): Sr-Nd isotopic constraints. Gondwana Res 5:287–305
Dodson MH (1973) Closure temperature in cooling geochronological and petrological systems. Contrib Mineral Petrol 40:259–274
Durand C, Boulvais P, Marquer D, Rossy M (2006) Stable isotope transfer in open and closed system across chemically contrasted boundaries: metacarbonate–granitoid contacts in the Quérigut magmatic complex (Eastern Pyrenees, France). Journal of Geological Society London 163:827–836
Eiler JM, Baumgartner LP, Valley JW (1992) Intercrystalline stable isotope diffusion: a fast grain boundary model. Contrib Mineral Petrol 112:543–557
Eiler JM, Valley JW, Baumgartner LP (1993) A new look at stable isotope thermometry. Geochim Cosmochim Acta 57:2571–2583
Farver JR, Yund RA (1991) Oxygen diffusion in quartz: dependence on temperature and water fugacity. Chem Geol 90:55–70
Fernandez AN, Gasquet DR (1994) Relative rheological evolution of chemically contrasted coeval magmas: example of the Tichka plutonic complex (Morocco). Contrib Mineral Petrol 116:316–326
Fourcade S, Allègre CJ (1981) Trace element behavior in granite genesis—a case study: the calc-alkalic plutonism association from the Querigut complex (Pyrénées, France). Contrib Mineral Petrol 76:177–195
Gasquet D (1991) Genèse d'un pluton composite tardi-hercynien. Le massif du Tichka, Haut Atlas Occidental (Maroc). PhD dissertation, Université de Nancy I, France
Gasquet D (1992) Mise en évidence d'intrusions emboîtées dans le Massif du Tichka (Haut -Atlas occidental, Maroc). CR Acad Sci Paris 314:931–936
Gasquet D, Leterrier J, Mrini Z, Vidal P (1992) Petrogenesis of the Hercynian Tichka plutonic complex (Western High Atlas, Morocco): trace element and Rb-Sr and Sm-Nd isotopic constraints. Earth Planet Sci Lett 108:29–44
Gasquet D, Stussi JM, Nachit H (1996) Les granitoïdes hercyniens du Maroc, dans le cadre de l'évolution géodynamique régionale. Bull Soc Géol France 167 :517–528.
Gazis CA, Lanphere M, Taylor HP Jr, Gurbanov A (1995) $^{40}Ar/^{39}Ar$ and $^{18}O/^{16}O$ studies of the Chegem ash-flow caldera and the Eldjurta granite: cooling of two late Pliocene igneous bodies in the Greater Caucasus Mountains, Russia. Earth Planet Sci Lett 134:377–391
Giletti BJ (1986) Diffusion effects on oxygen isotope temperatures of slowly cooled igneous and metamorphic rocks. Earth Planet Sci Lett 77:218–228
Giletti BJ, Anderson TF (1975) Studies in diffusion II: oxygen in phlogopite mica. Earth Planet Sci Lett 28:225–233
Giletti BJ, Yund RA (1984) Oxygen diffusion in quartz. J Geophys Res 89:4039–4046
Glazner AF, Bartley JM, Coleman DS, Gray W, Taylor RZ (2004) Are plutons assembled over millions of years by amalgamation from small magma chambers? GSA Today 14:4–11
Gregory RT, Taylor HPJr (1981) An oxygen isotope profile in a section of Cretaceous oceanic crust, Samail ophiolite, Oman: evidence for $\delta^{18}O$ buffering of the océans by deep (>5 km) seawater-hydrothermal circulation at mid-ocean ridges. J Geophys Res 86:2737–2755
Gregory RT, Criss RE, Taylor HPJr (1989) Oxygen isotope exchange kinetics of mineral pairs in closed and open systems: applications to problems of hydrothermal alteration of igneous rocks and precambrian iron formations. Chem Geol 75:1–42
Hess JC, Lippolt HJ, Gurbanov AG, Michalski I (1993) The cooling history of the late Pliocene Eldzhurtinskiy granite (Caucasus, Russia) and the thermochronological potential of grain-size/age. Earth Planet Sci Lett 117:393–406
Jendrzejwski N, Javoy M, Trull T (1996) Mesures quantitatives de carbone et d'eau dans les verres basaltiques naturels par spectroscopie infrarouge. Partie II: l'eau. CR Acad Sci Paris 322:735–742
Johannes W, Holtz F (1996) Petrogenesis and experimental petrology of granitic rocks. Springer, Berlin, p 335
Kohn MJ, Valley JW (1998) Oxygen isotope geochemistry of the amphiboles: Isotope effects of cation substitutions in minerals. Geochim Cosmochim Acta 62:1947–1958
Lagarde JL, Roddaz B (1983) Le massif plutonique du Tichka (Haut Atlas occidental, Maroc): un diapir syntectonique. Bull Soc Géol France 7:389–395
Lapique F, Champenois M, Cheilletz A (1988) Un analyseur vidéographique interactif: développement et applications. Bull Mineral 111:679–687
Lawrence JR, Taylor HPJr (1971) Deuterium and oxygen-18 correlation: clay minerals and hydroxides in quaternary soils compared to meteoric waters. Geochim Cosmochim Acta 35:993–1003
Lécuyer C, Fourcade S (1991) Oxygen isotope evidence for multistage hydrothermal alteration at a fossil slow-spreading center: the Silurian Trinity ophiolite. Chem Geol 87:231–246
Lécuyer C, Reynard B (1996) High-temperature alteration of oceanic gabbros by seawater (Hess Deep, Ocean Drilling Program Leg 147): evidence from oxygen isotopes and elemental fluxes. J Geophys Res 101:15883–15897
Matzel JEP, Bowring SA, Miller RB (2006) Time scales of pluton construction at differing crustal levels: examples from the Mount Stuart and Tenpeak intrusions, North Cascades. Washington GSA Bul 118:1412–1430
McConnell JDC (1995) The role of water in oxygen isotope exchange in quartz. Earth Planet Sci Lett 136:97–107
Menand T (2011) Physical controls and depth of emplacement of igneous bodies: a review. Tectonophysics 500:11–19
Menand T, Annen C, de Saint Blanquat M (2015) Rates of magma transfer in the crust: Insights into magma reservoir recharge and pluton growth. Geology 43:199–202
Paterson MS (1982) The determination of hydroxyl by infrared absorption in quartz, silicate glasses and similar materials. Bull Mineral 105:20–29

Paterson MS (1986) The thermodynamics of water in quartz. Phys Chem Minerals 13:245–255

Pitcher WS (1983) Granite: typology, geological environment and melting relationships. In: Atherton MP, Gribble CD (eds) Migmatites, melting and metamorphism. Shiva Pub, Nantwich, pp 277–287

Price PH, Slack MR (1954) The effect of latent heat on numerical solutions of heat flow equations. Br J Appl Phys 5:285–287

Ruano SM, Both RA, Golding SD (2002) A fluid inclusion and stable isotope study of the Moonta copper-gold deposits, South Australia: evidence for fluid immiscibility in a magmatic hydrothermal system. Chem Geol 192:211–226

Schactner R, Sockel HG (1977) Study in diffusion in quartz by activation analysis. In: Wood J, Lindquist O, Helgeson C, Vannerburg NG (eds) Reactivity of solids. Proc. 8th Int'1 Symp, pp 605–609

Scott GB, Vogel TA (1980) The origin of the acidic and basic rocks of the Tichka Massif, Morocco, based on rare earth elements. Contrib Mineral Petrol 75:89–95

Simon L, Lécuyer C (2005) Continental recycling: the oxygen isotope point of view. Geochem Geophys Geosyst. doi:10.1029/2005GC000958

Simons B, Shail RK, Andersen JCØ (2016) The Petrogenesis of the Early Permian Variscan granites of the Cornubian Batholith—lower plate post-collisional peraluminous magmatism in the Rhenohercynian Zone of SW England. Lithos 260:76–94

Smith DR, Noblett J, Wobus RA, Unrush D, Douglass J, Beane R, Davis C, Goldman S, Kay G, Gustavson B, Saltoun B, Stewart J (1999) Petrology and geochemistry of late-stage intrusions of the A-type, mid-Proterozoic Pikes Peak batholith (Central Colorado, USA): implications for petrogenetic models. Precamb Res 98:271–305

Stüwe K (1995) Thermal buffering effects at the solidus. Implications for the equilibration of partially melted metamorphic rocks. Tectonophysics 248:39–51

Tartèse R, Boulvais P (2010) Differentiation of peraluminous leucogranites "en route" to the surface. Lithos 114:353–368

Tartèse R, Poujol M, Ruffet G, Boulvais P, Yamato P, Kosler J (2011) New U-Pb zircon and $^{40}Ar/^{39}Ar$ muscovite age constraints on the emplacement of the Lizio syn-tectonic granite (Armorican Massif, France). CR Geosci 343:443–453

Taylor HPJr (1968) The oxygen isotope geochemistry of igneous rocks. Contrib Mineral Petrol 19:1–71

Taylor HPJr (1977) Water/rock interactions and the origin of H2O in granitic batholiths. J Geol Soc Lond 133:509–558

Taylor HPJr (1978) Oxygen and hydrogen isotope studies of plutonic granitic rocks. Earth Planet Sci Lett 38:177–210

Taylor HPJr (1980) The effects of assimilation of country rocks by magmas on 18O/16O and 87Sr/86Sr systematics in igneous rocks. Earth Planet Sci Lett 47:243–254

Taylor HPJr (1988) Oxygen, hydrogen, and strontium isotope constraints on the origin of granites. Trans R Soc Edinb 79:317–338

Taylor HP Jr, Sheppard SMF (1986) Igneous rocks: I. Processes of isotopic fractionation and isotope systematics. In: Valley JW, Taylor HP Jr, O'Neil JR (eds) Stable isotopes in high temperature geological processes, vol 16. Mineral Society of America, Washington, DC, pp 227–271

Termier H, Termier G (1971) Le massif granito-dioritique du Tichka (Haut Atlas occidental, Maroc). 1, Les régions et les terrains. Notes et Mémoires du Service Géologique du Maroc, Service Géologique du Maroc, Rabat, n° 216, 240 pp

Turcotte D, Schubert G (1982) Geodynamics. Wiley, New York, 450 pp

Van de Flierdt T, Hoernes S, Jung S, Masberg F, Hoffer E, Schaltegger U, Friedrichsen H (2003) Lower crutsal meltong and the role of open-system processes in the genesis of syn-orogenic quartz diorite-granite-leucogranite assocaitins: constraints from Sr-Nd-O isotopes from bandombaai Complex, Namibia. Lithos 67:205–226

Vielzeuf D, Pin C (1989) Geodynamic implications of granulitic rocks in the Hercynian belt. In: Daly JS, Cliff RA, Yardley BWD (eds) Evolution of metamorphic belts, vol 43. Geological Society Special Publication, pp 343–348

Vogel TA, Walker BM (1975) The Tichka Massif, Morocco—an example of contemporaneous acidic and basic plutonism. Lithos 8:29–38

Wang X, Griffin WL, O'Reilly SY, Zhou XM, Xu XS, Jackson SE, Pearson NJ (2002) Morphology and geochemistry of zircons from late Mesozoic igneous complexes in coastal SE China: implications for petrogenesis. Mineral Mag 66:235–251

Weiss D, Demaiffe D, Cauet S, Javoy M (1987) Sr, Nd, O and H isotopic ratios in Ascension Island lavas and plutonic inclusions; cogenetic origin. Earth Planet Sci Lett 82:255–268

Wickham SM, Taylor HPJr (1985) Stable isotopic evidence for large-scale seawater infiltration in a regional metamorphic terrane; the trois Seigneurs massif, Pyrenees, France. Contrib Mineral Petrol 91:122–137

Wickham SM, Taylor HPJr (1987) Stable isotope constraints on the origin and depth of penetration of hydrothermal fluids associated with Hercynian low-pressure regional and crustal anatexis in the Pyrenées. Contrib Mineral Petrol 95:255–268

Wiebe RA, Collins WJ (1998) Depositional features and stratigraphic sections in granitic plutons: implications for the emplacement and crystallization of granitic magma. J Struct Geol 20:1273–1289

Wu FY, Jahn BJ, Wilde SA, Lo CH, Yui TF, Lin Q, Ge WC, Sun DY (2003) Highly fractionated I-type granites in NE China (II): isotopic geochemistry and implications for crustal growth in the Phanerozoic. Lithos 67:191–204

Zak K, Pudilova M, Breiter K (2005) Oxygen isotope study of the highly fractionated Podlesi granite system, Krusne hory Mts., Czech Republic. Bull Geosci 80:139–143